Arabian Journal of Chemistry (2019) **12**, 5200–5211

King Saud University

Arabian Journal of Chemistry

www.ksu.edu.sa
www.sciencedirect.com

ORIGINAL ARTICLE

Acid functionalized-nanoporous carbon/MnO_2 composite for removal of arsenic from aqueous medium

Shahin Pathan [a,b,*], **Nancy Pandita** [a], **Nand Kishore** [c]

[a] *Department of Chemical Sciences, Sunandan Divatia School of Science, NMIMS University, Vile Parle (West), Mumbai 400056, India*
[b] *K.J. Somaiya Institute of Engineering and Information Technology, Sion(E), Mumbai 400022, India*
[c] *Department of Chemistry, Indian Institute of Technology Bombay, Powai, Mumbai 400076, India*

Received 6 September 2016; accepted 15 December 2016
Available online 31 December 2016

KEYWORDS

Nanoporous carbon;
MnO_2;
Adsorption;
Aqueous medium

Abstract Nanoporous carbon (NPC) structures synthesized from grass clippings mown at yard were acid functionalized and coated with manganese oxide nanoparticles at room temperature. The synthesized composite was characterized by FTIR, XRD, BET, TEM, TGA and XPS. Characterization results showed formation of acid functionalized nanoporouscarbon/MnO_2 (Af-NPC/MnO_2) composite which was amorphous in nature. Af-NPC/MnO_2 was further explored for removal of As(III) and As(V) from aqueous medium. Effects of factors such as pH, contact time, initial concentration and interfering ions on adsorption of arsenic by Af-NPC/MnO_2 were studied in detail. The mechanism of adsorption was also studied using experimental data determined. The kinetic study indicated that removal of arsenic follow pseudo second order kinetics and the experimental equilibrium data fitted better in Langmuir isotherm model with maximum monolayer adsorption capacity of 8.85 mg/g and 9.43 mg/g for As(III) and As(V), respectively. The removal rate of arsenic was found to be very fast compared to other adsorbents. The results of this study imply that Af-NPC/MnO_2 is an efficient adsorbent for removal of As(III) and As(V) from aqueous medium.
© 2016 The Authors. Production and hosting by Elsevier B.V. on behalf of King Saud University. This is an open access article under the CC BY-NC-ND license (http://creativecommons.org/licenses/by-nc-nd/4.0/).

* Corresponding author at: K.J. Somaiya Institute of Engineering and Information Technology, Ayurvihar Complex, Near Everard Nagar, Sion (East), Mumbai 400022, India.
E-mail address: shaheen@somaiya.edu (S. Pathan).
Peer review under responsibility of King Saud University.

Production and hosting by Elsevier

http://dx.doi.org/10.1016/j.arabjc.2016.12.011
1878-5352 © 2016 The Authors. Production and hosting by Elsevier B.V. on behalf of King Saud University.
This is an open access article under the CC BY-NC-ND license (http://creativecommons.org/licenses/by-nc-nd/4.0/).

1. Introduction

Water is one of the most essential and precious natural resources on earth. Contamination of water with toxic substances due to rapid urbanization has become a worldwide cause of concern. Among these substances arsenic occupies topmost position in the priority list of hazardous substances given by ATSDR (2015). Many toxic effects of arsenic contamination have been already reported in countries such as Bangladesh and India (West Bengal). Among 21 countries affected by ground water arsenic contamination the largest population at risk is in Bangladesh followed by West Bengal in India (Mohan and Pittman Jret, 2007). In West Bengal alone, 26 million people are potentially at risk from drinking arsenic-contaminated water (above 0.01 mg/L) (Chakraborti et al., 2009). Major sources of ground water arsenic contamination are natural weathering reactions; apart from this industrial waste and municipal waste also pollute water with arsenic (Lone et al., 2008).

Arsenic is said to be synonymous to toxicity and also carcinogenic (Smith et al., 2000). Hence this toxic metalloid should be removed from drinking water. There are a number of methods developed for removal of arsenic from water such as electrolysis, chemical precipitation, oxidation–reduction, ion exchange and adsorption on suitable sorbents. But among all these methods, use of suitable adsorbent is always preferred due to better removal capacity and reusability. Many sorbents have been studied for adsorption of arsenic such as biomass derived activated carbon (Budinova et al., 2009), biological materials (Giri et al., 2013; Kamala et al., 2005), biomass based composites (Shengsen et al., 2015;), laterite (De and Maiti, 2012), zeolite (Meltem and Aysegul, 2014), metal oxides and nanomaterials (Gupta et al., 2005; Hristovski et al., 2007). But many of these adsorbents have limitations such as slow rate of adsorption and low As(III) removal efficiency (Budinova et al., 2009; Gupta et al., 2005; Meltem and Aysegul, 2014; Shengsen et al., 2015; Zhang et al., 2010b; Yao et al., 2014). Arsenic actually occurs in two forms i.e. As(III) (arsenite) and an oxyacid As(V) (arsenate) (De and Maiti, 2012). As(III) exists as H_3AsO_3 a neutral species at ground water pH which is four times more toxic than As(V) (De and Maiti, 2012). Hence there is a need to synthesize an adsorbent with fast removal rate and better adsorption efficiency for not only As(V) but also As(III). As carbon nanomaterials in various forms are being widely studied for environmental remediation due to their useful properties such as high surface area and good mechanical strength (Mishra and Ramaprabhu, 2011; Mojtaba et al., 2014: Ntim and Mitra, 2011), and in the present study acid functionalized nanoporous carbon (Af-NPC) was synthesized from grass mown at yards and coated by MnO_2 nanoparticles. This composite (Af-NPC/MnO_2) was then studied as an adsorbent for removing both As(III) and As(V) from aqueous medium. There are very few studies reported in the literature indicating use of MnO_2 based composite as adsorbent for arsenic removal. The current study reports first time use of MnO_2 composite with biomass derived nanoporous carbon for removal of arsenic from aqueous medium. Use of biomass based precursor for synthesis of nanoporous carbon reduces cost of synthesis.

Since As(III) is neutral it is difficult to adsorb on various sorbents. In order to increase removal of As(III) by adsorption As(III) is first oxidized to negatively charged As(V) in a separate step using various oxidizing agents (Shihabudheen et al., 2009) and then allowed to react with adsorbents. There are numerous oxidizing agents used for this purpose such as Ozone, chlorine and UV radiations but these oxidizing agents have limitations such as low reactivity, cost and production of harmful by-products. The most feasible oxidant is potassium permanganate for oxidation of arsenite since it does not produce harmful byproducts (Jiang, 2001). Hence in the present study in order to eliminate extra step of oxidizing As(III) in the process of arsenic removal by adsorption, acid functionalized nanoporous carbon (Af-NPC) was synthesized from grass and coated by MnO_2 nanoparticles. These MnO_2 nanoparticles bring about oxidation of As(III) to As(V) on the surface of Af-NPC/MnO_2, which is subsequently adsorbed on the surface of same adsorbent.

2. Experimental details

2.1. Synthesis of Af-NPC/MnO_2 nanocomposite

Acid functionalized nanoporous carbon (Af-NPC) was synthesized from grass clippings mown at yards due to availability and to reduce cost of synthesis. Synthesis was done by pyrolysis of grass in a tube furnace as described earlier (Shahin and Nancy, 2016). In brief yard grass clippings were powdered and dried at 95 °C for 6 h. After drying grass powder was impregnated with $FeCl_3{\cdot}6H_2O$ solution in acetone, which was air-dried at room temperature. This mixture was pyrolyzed in a tube furnace in flowing nitrogen with a flow rate of 30 cc/min at 800 °C for 2 h. The obtained carbon products were immersed and sonicated in aqua regia (HNO_3: H_2SO_4 = 1:3) for 2 h and kept overnight for functionalization of carbon surface with different oxygen containing functional groups. Treatment with acid also removes catalysts from NPC. After acid treatment and purification carbon products were washed several times with double distilled water to remove acid and dried at 100 °C. Af-NPC was coated with MnO_2 using redox reaction (Wang et al., 2007). In order to coat Af-NPC with 25% loading of MnO_2 0.2 g of Af-NPC was first sonicated in 30 mL deionized water for 15 min at room temperature. Then 0.17 g of Mn (II) chloride was dissolved in 5 mL of water and added to Af-NPC water mixture with continuous stirring. After adding $MnCl_2$, 3.5 mL of 0.13 M $KMnO_4$ solution was added to the same solution drop wise under continuous stirring. The solution turned dark brown indicating precipitation of MnO_2. This suspension was further heated to 80 °C for 1 h. The Af-NPC coated with MnO_2 (Af-NPC/MnO_2) composite was then filtered and washed repeatedly with deionized water and dried at 105 °C.

Af-NPC/MnO_2 composites with different loadings of MnO_2 were prepared and tested for arsenic removal. Percentage loading of MnO_2 in composites prepared was determined by heating composite in a furnace at 378 °C in the presence of air. As per TGA analysis (Fig. 2e) heating at 378 °C completely removes carbon from composite leaving behind residue of MnO_2. The residue left was weighed to calculate percentage loading of MnO_2 on the surface of Af-NPC/MnO_2. The composite Af-NPC/MnO_2 with 25% loading was found to be efficient for removal of arsenic and hence further adsorption study was done using composite with 25% loading of MnO_2.

2.2. Structural and physicochemical characterization

Fourier Transform Infrared Spectroscopy (FTIR) was carried out using Jasco, FTIR 460 Plus spectrometer with TGS detector, and the spectra were recorded between 4000 cm^{-1} and 400 cm^{-1}. For FTIR analysis Af-NPC/MNO_2 composite was treated with 10 mg/L As(III) and As(V) aqueous solutions separately for 1 h at pH 6. After adsorption composite was filtered and dried at 100 °C before FTIR analysis. X-ray diffraction (XRD) patterns were obtained on a Rigaku D/MAX 2500 diffractometer with Cu K alpha radiation (λ = 1.5418 Å) using a generator voltage of 40 kV and a generator current of 250 mA. The surface area and porosity characteristics were obtained by performing N_2 sorption/desorption isotherms on a Micromeritics ASAP 2020 V3.00 H volumetric adsorption system at −195.690 °C. Transmission electron microscopy (TEM)

images were collected on a Philips, CM 200 transmission electron microscope with acceleration voltage of 200 kV. TGA analysis was carried out using PERKIN ELMER, Diamond TG/DTA in the presence of air. Surface properties of Af-NPC/MnO_2 were determined by X-ray photoelectron spectroscopy on Kratos Analytical, Axis Supra. All samples were dried in vacuum at room temperature before XPS analysis. Zeta potential of Af-NPC/MnO_2 was determined by Malvern Zeta Analyzer in water between pH ranges of 2–10.

2.3. Adsorption experiments

All chemicals used in the experiments were of analytical grades. As(III) and As(V) stock solutions of 1000 mg/L were prepared by mixing appropriate amounts of AR grade sodium meta arsenite ($NaAsO_2$) and sodium arsenate ($Na_2HAsO_4{\cdot}7H_2O$) respectively in deionized water. Working solutions of desired arsenic concentrations were freshly prepared by diluting stock solutions.

MnO_2, Af-NPC and Af-NPC/MnO_2 were tested separately for removal of both As(III) and As(V). For this 0.5 mg/L arsenic solution was mixed with 1 g/L of different adsorbents for about 1 h at 150 rpm and pH 6.5. Further study was done with Af-NPC/MnO_2 as arsenic removal efficiency of it was more than MnO_2 and Af-NPC. For the pH dependent removal efficiency the adsorption experiments were conducted by mixing 10 mL of 1 mg/L arsenic solution at different pH (4–10) ranges with 1 g/L of Af-NPC/MnO_2 for about 1 h at 150 rpm and room temperature. The pH of the reaction mixture was adjusted with aqueous solution of 0.1 N HCl and 0.1 N NaOH. In order to assess the adsorption kinetics, batch adsorption experiments were carried out by mixing 1 g/L Af-NPC/MnO_2 to 10 mL of arsenic solutions with different concentrations (1, 5 and 10 mg/L) for predetermined time intervals (5, 10, 15, 20, 30, 60, 120 min) keeping other parameters same. The adsorption of arsenic for different initial concentrations (0.6–10 mg/L) was investigated on Af-NPC/MnO_2 at room temperature. For this 10 mL of arsenic solutions at different concentrations was mixed with 1 g/L of Af-NPC/MnO_2 for an adsorption period of 1 h at pH 6. The above mixtures were kept under continuous shaking at room temperature and 150 rpm. Arsenic removal efficiency of Af-NPC/MnO_2 was also evaluated in the presence of salts by increasing concentration of NaCl and Na_2SO_4 from 0 to 0.1 M with initial arsenic concentration of 1 mg/L and keeping other parameters constant. Removal efficiency of composite was also accessed for ground water samples spiked with 1 mg/L of As(III) and As (V) solutions under the same conditions of pH, time and rotation, to find effect of natural environment on removal efficiency of adsorbent. All the samples after adsorption were filtered through 0.45 μm syringe filters. Initial and final concentrations were determined by inductively coupled plasma-atomic emission spectrometer (ICP-AES, ARCOS from M/s. Spectro, Germany).

The recycling capacity of Af NPC/MnO_2 was investigated by performing three succeeding cycles of adsorption–desorption. As adsorption of As(III) and As(V) decreases with increase in pH (Fig. 4b), 0.1 N NaOH was used for desorption of arsenic from Af-NPC/MnO_2 after each cycle of adsorption. In the desorption process, 30 mg of used Af-NPC/MnO_2 composite was dispersed into 10 mL of 0.1 N NaOH and rotated on shaker for 20 min. All the samples were filtered through 0.45 μm membrane filters and thoroughly washed several times with deionized water after each cycle of desorption. The reconstituted adsorbents were reused for adsorption in the next cycles. The initial concentration of both arsenic species used for desorption experiments was 1 mg/L.

All the adsorption experiments were performed in triplicates and the average values are reported here. The equilibrium arsenic adsorption capacity q_e (mg/g) and percentage removal efficiency (% R) were calculated by Eqs. (1) and (2) respectively.

$$q_e = \frac{(C_0 - C_e)V}{M} \tag{1}$$

$$\%\ R = \frac{C_0 - C_e}{C_0} \times 100 \tag{2}$$

where C_0 and C_e are the initial and final equilibrium concentrations of arsenic ions (mg/L) in aqueous solution, V is the total volume of solution (L) and M is the adsorbent mass (g).

3. Results and discussion

3.1. Characterization of Af-NPC/MnO_2

3.1.1. FTIR analysis

Fig. 1 shows FTIR spectra of Af-NPC/MnO_2 before and after adsorption of As(III) and As(V). In order to comprehend bonding of MnO_2 on Af-NPC/MnO_2 the IR spectral analysis was focused on two characteristic peaks. A peak that usually appears around 517 cm^{-1} in pure MnO_2 (Huang et al., 2014) has appeared at 568 cm^{-1} in the IR spectrum of composite. The shift of this peak toward higher frequency could be

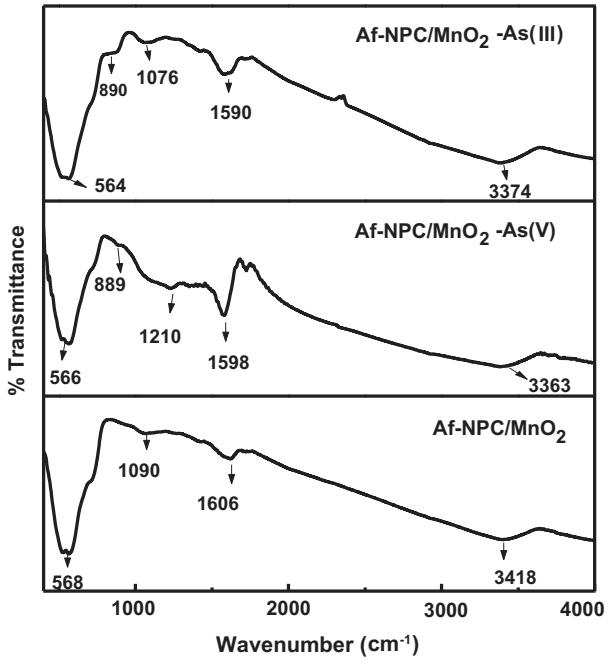

Figure 1 FTIR spectrum of Af-NPC/MnO_2 before and after adsorption of As(V) and As(III) from aqueous medium at pH 6.

attributed to strong bond between the MnO_2 and Af-NPC. The second peak is the band assigned to C═O stretching vibration of ─COOH. This peak usually appears at 1717 cm^{-1} for Af-NPC (Shahin and Nancy, 2016) which has shifted towards lower wave number 1606 cm^{-1} after loading of MnO_2 in Af-NPC/MnO_2, indicating interaction between MnO_2 nanoparticles and the carbon through carboxyl group by chemisorptions of carboxylate ions (Singh et al., 2011).

The shifts in vibrational frequencies of ─OH group were observed from 3418 cm^{-1} to 3374 cm^{-1} and 3363 cm^{-1} after adsorption of As(III) and As(V) respectively in Fig. 1, which indicates interaction of OH groups with arsenic ions. Changes in vibrational frequencies of C─O stretching vibration from 1090 cm^{-1} to 1076 cm^{-1} and 1210 cm^{-1} after adsorption of arsenic imply involvement of C─O groups as well in adsorption of arsenic on the surface of Af-NPC/MnO_2. Peaks at 889 cm^{-1} and 890 cm^{-1} were of As(V)─O stretching frequencies (Xiu et al., 2010). The presence of As(V) on the surface of composite after adsorption of As (III) from aqueous medium confirms that As(III) was oxidized to As(V) on the surface of Af-NPC/MnO_2. No major shifts were seen in vibrational frequency of ─OH and ─CO groups, which proves that bonding of arsenic with Af-NPC/MnO_2 was not very strong. Some minor shifts were seen in frequencies due to changes in electronic atmosphere after adsorption of arsenic.

3.1.2. XRD analysis

XRD patterns of Af-NPC, MnO_2 and Af-NPC/MnO_2 composite were determined to get an insight into molecular structure of these compounds. XRD pattern of only Af-NPC (Fig. S1a, supplementary information), shows two broad peaks around 2θ° values of 24.5° and 44° indicating the presence of graphitic carbon. There were no well defined peaks seen in XRD pattern of only MnO_2 (Fig. S1b, supplementary information) which proves amorphous nature of manganese oxide. In XRD graph of composite (Fig. S1c, supplementary information) it is not possible to distinguish peaks of Af-NPC due to incorporation of MnO_2. The broad diffraction peaks of Af-NPC and Af-NPC/MnO_2 indicate that the products were poorly crystallized and amorphous in nature (Huang et al., 2014; Wang et al., 2005).

3.1.3. BET analysis

Nitrogen adsorption–desorption isotherms and pore size distribution curve of composite after MnO_2 loading are shown in Fig. 2a and b respectively. Af-NPC/MnO_2 showed Type IV adsorption–desorption isotherm with H3 type hysteresis loop (Thommes, 2010; Patel et al., 2013; Lee and Pyun, 2007) indicating the presence of mesoporosity.

The Brunauer-Emmett-Teller specific surface area calculated from physisorption isotherm was 633 m^2/g corresponding to Af-NPC/MnO_2 with 25% loading of MnO_2 by wt. The decrease in surface area compared to 1013.71 m^2/g surface area of Af-NPC previously reported (Shahin and Nancy, 2016) can be attributed to blocking of pores by MnO_2 particles. The composite retains porous structure as surface area did not reduce much even after loading of MnO_2. The pore diameter and pore volume of composite were 2.6 nm and 0.414 cm^3/g respectively.

3.1.4. TEM analysis

TEM micrographs of Af-NPC and Af-NPC/MnO_2 are presented in Fig. 2c and d respectively. Formation of MnO_2 nanopetals on the surface of Af-NPC can be clearly seen in Fig. 2d. The average size of MnO_2 particles was 24 nm in width and 80 nm in length.

3.1.5. TGA analysis

The thermal stability of Af-NPC/MnO_2 was measured by thermo gravimetric analysis (TGA). Fig. 2e shows the TGA profiles of Af-NPC and Af-NPC/MnO_2. The TGA profile of Af-NPC can be divided into three segments. The first segment indicates slow loss of carbon till 420 °C due to oxidation of defected carbon produced during acid functionalization. In the second segment rapid loss of carbon is seen till 560 °C, followed by flat plateau. The TGA profiles of Af-NPC/MnO_2 can be divided into four segments. The first segment is from room temperature to 300 °C corresponding to the slow loss of carbon due to oxidation of defected carbon. Second segment ranges from 300 °C to 378 °C indicating major and rapid loss of carbon. The weight loss beyond 378 °C can be attributed to the slow decomposition of MnO_2 to Mn_2O_3 at high temperature. Beyond 500 °C the weight remains constant and profiles became flat plateau. Thus, the content of MnO_2 in this sample of composite based on the TGA profiles was 37.8 wt%.

3.1.6. XPS analysis

XPS studies were performed in order to evaluate surface characteristics, chemical composition and chemical state of elements present on the surface of Af-NPC and Af-NPC/MnO_2 (before and after adsorption of arsenic). The wide XPS spectrum of Af-NPC and Af-NPC/MnO_2 (Fig. S2 a and b, supplementary information) shows two prominent peaks corresponding to C and O at 288 eV and 533 eV respectively. A third relatively small peak attributed to Mn at 648 eV was seen in Af-NPC/MnO_2.

Fig. 3a shows the XPS spectrum of O1s levels. Deconvolution of O1s peak of Af-NPC indicated the presence of three peaks at binding energies 530.40 eV, 531.6 eV and 533 eV which may be assigned to H─O─C═O, C═O and ─C─OH respectively. Shifts in binding energies were observed to lower values in O1s level of Af-NPC/MnO_2 after coating with MnO_2 indicating formation of new bonding between MnO_2 and Af-NPC through oxygen containing functional groups. The peak at 529.7 eV in composite was caused by bonding between Mn and O atoms (Qu et al., 2009; Lee et al., 2014). The C1 s spectra in Fig. 3b show the presence of two peaks at 284.8 eV and 288.9 eV representing sp2-hybridized graphitic carbon and carbonyl group respectively in Af-NPC. The B.E 288.9 eV of Af-NPC reduces to 288.6 eV in Af-NPC/MnO_2 after coating of MnO_2. In Fig. 3d two peaks at 653.6 eV and 641.8 eV can be assigned to Mn $2p_{3/2}$ and Mn $2p_{1/2}$ respectively. The energy gap between these two peaks is 11.8 eV, similar to the spin–orbit separation of $2p_{3/2}$ and $2p_{1/2}$ indicating formation of MnO_2 (Sreeprasad et al., 2011) on the surface of composite. The As3d levels were observed at B.E 45 eV in both As(V) and As(III) adsorbed Af-NPC/MnO_2 as shown in Fig. 3d and e respectively. The peak at B.E 45 eV implies the presence of AsO_4^{3-} species on the surface of Af-NPC/MnO_2 (Zhang et al., 2010a; Wagner et al., 1979), which indicates the presence of As(V) on the surface of composite after

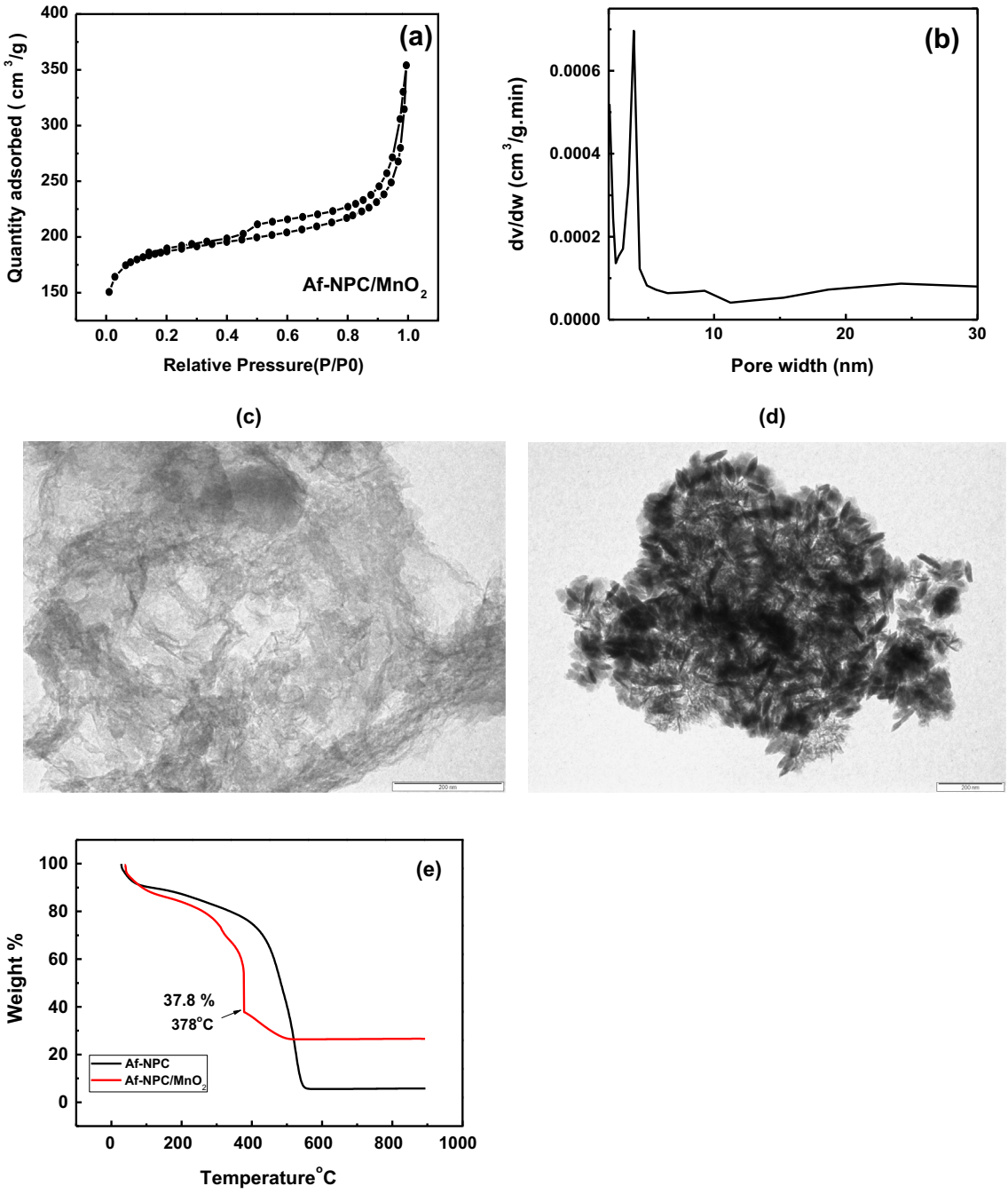

Figure 2 (a) and (b) N_2 adsorption–desorption isotherm and pore size distribution curve of Af-NPC/MnO_2 composite respectively, (c) TEM micrograph of Af-NPC, (d) TEM micrograph of Af-NPC/MnO_2 (e) TGA profile of Af-NPC and Af-NPC/MnO_2 in the presence of air.

adsorption of As(III) or As(V) from aqueous medium. Thus based on XPS results we can conclude that As(III) was oxidized to As(V) by MnO_2 on the surface of Af-NPC/MnO_2 during the process of adsorption. The oxidation of As(III) to As(V) by manganese oxide was shown by many researchers with redox reactions involved (Driehaus et al., 1995).

3.1.7. pHpzc

The pH of zero point charge (pHpzc) of Af-NPC and Af-NPC/MnO_2 was found to be around 2.5 and 3.5, respectively. Thus, Af-NPC and Af-NPC/MnO_2 have positive surface charge at pH < pHpzc and negative surface charge at pH > pHpzc. It has been observed that the pHpzc of Af-NPC/MnO_2 increases upon binding of MnO_2 nanoparticles.

3.2. Adsorption study

3.2.1. Removal of arsenic by different adsorbents

The percentage removal efficiency of As(III) and As(V) by Af-NPC/MnO_2 was more than that of Af-NPC and MnO_2

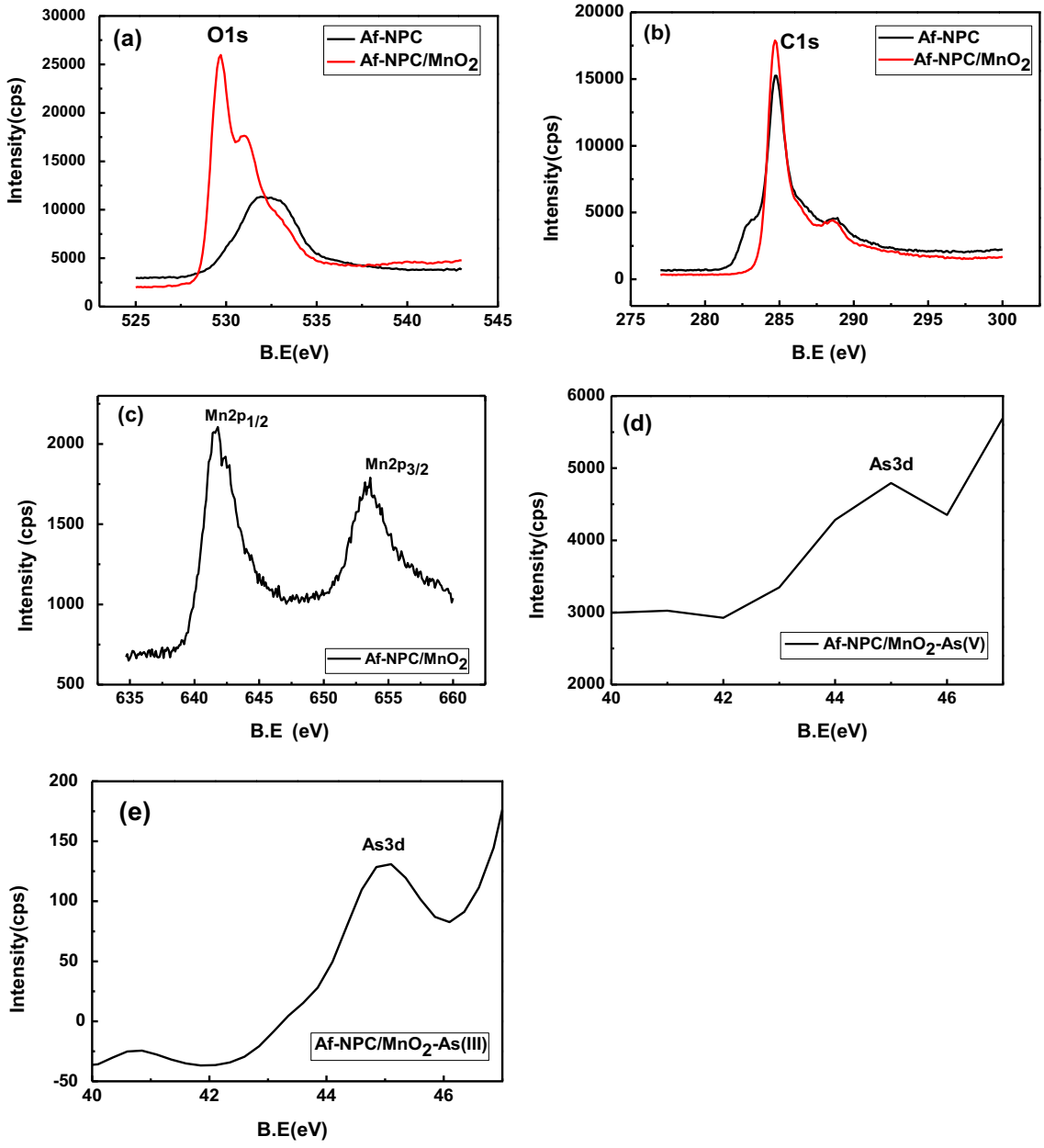

Figure 3 (a) XPS response of O1s core levels of Af-NPC and Af-NPC/MnO_2, (b) XPS response of C1s core levels of Af-NPC and Af-NPC/MnO_2, (c) Mn 2p core levels in Af-NPC/MnO_2 (d) and (e) As3d core levels in Af-NPC/MnO_2 after adsorption of As(V) and As(III) respectively.

(Fig. 4a). Percentage removal efficiency of Af-NPC/MnO_2 for As(III) was 98% and that of Af-NPC and MnO_2 was 35% and 45% respectively. Higher removal efficiency of composite may be attributed to oxidation of As(III) to negatively charged As (V) oxyanion by MnO_2 on the surface of Af-NPC/MnO_2 and subsequent adsorption on the surface of composite. Availability of more number of active functional groups (—OH) on the surface of composite for adsorption of arsenic might be responsible for increasing As(V) removal efficiency by the composite.

3.2.2. Effect of pH

There was not much variation observed in percent removal of arsenic between pH 4 and 7 by Af-NPC/MnO_2 (Fig. 4b). The pHpzc of composite was 3.5; hence, the surface of composite was negative above pH 3.5. At pH less than 7 As(V) also exists as negatively charged monovalent species $H_2AsO_4^-$. Hence these negatively charged species of arsenic must be adsorbed by anion exchange process with hydroxylated surface of Af-NPC/MnO_2. Equilibrium pH of aqueous medium increases after adsorption of arsenic which indicates release of OH^- ions

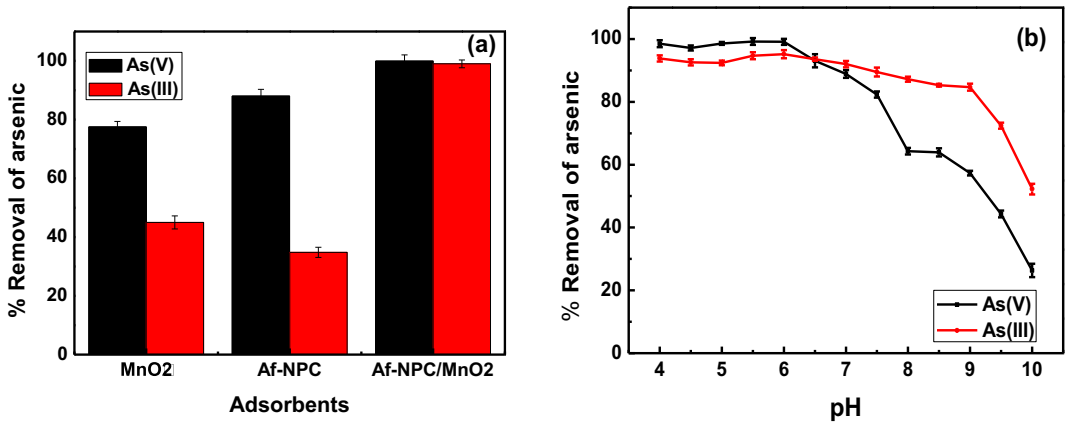

Figure 4 (a) % Removal efficiency of As(III) and As(V) by different adsorbents at initial concentration of 0.5 mg/L and pH 6.5, (b) effect of pH on adsorption of As(III) and As(V) by Af-NPC/MnO_2 at room temperature.

and supports anion exchange mechanism of adsorption. In the pH range above 7 As(V) exists as $HAsO_4^{2-}$ but at the same time the OH^- ions were also increased in solution. The affinity of OH^- ions with carbon was more than $HAsO_4^{2-}$; hence, adsorption of As(V) decreases in alkaline medium due to competition with OH^- ions for adsorption sites. Since ground water pH lies between 6 and 8.5 further adsorption studies were carried out at pH 6.

3.2.3. Sorption kinetic studies

Sorption kinetic studies were conducted with Af-NPC/MnO_2 in batch mode using different initial concentrations of arsenic. Sorption kinetic data were analyzed by Lagergren pseudo first-order model and Ho's pseudo-second-order reaction rate models. Mathematical representations of these models are given in Eqs. (3) and (4) respectively (Dutta et al., 2015).

Lagergren pseudo first- order model

$$\frac{dq_t}{dt} = K_1(q_e - q_t) \tag{3}$$

Ho's pseudo-second-order equation:

$$\frac{dq_t}{dt} = K_2(q_e - q_t)^2 \tag{4}$$

where q_t is amount of adsorbate in mg/g sorbed on the sorbent surface at any time t. k_1 and k_2 are the first order rate constant (min^{-1}) and the second-order rate constant (g/mg min) of sorption respectively and t is the time (min). The initial adsorption rate (h) at $t = 0$ min can also be calculated from the t/q_t vs t plot, using following equation.

$$h = K_2 q_e^2 \tag{5}$$

Table 1 indicates that pseudo second order model fitted well for arsenic adsorption as regression coefficients are higher than first order kinetics and q_e values are in close agreement with the experimental values. Pseudo second order kinetics indicates that arsenic was adsorbed through chemisorption on the surface of Af-NPC/MnO_2 which implies that active functional groups present on the surface of Af-NPC/MnO_2 interact with arsenic. The equilibrium for arsenic adsorption was reached within 15–20 min (Fig. 5). At lower concentration of arsenic removal was faster. Table 2 shows the comparison of Af-NPC/MnO_2 with the other adsorbents from the literature with respect to equilibrium time, adsorption capacity and surface area. Af-NPC/MnO_2 has better adsorption capacity and faster removal rate compared to other adsorbents mentioned in Table 2, as the surface area of Af-NPC/MnO_2 is comparatively high.

3.2.4. Adsorption isotherms

Adsorption isotherms provide information about adsorption capacity and interaction of adsorbate molecules with adsorbent. The study also guides in designing proper adsorption system. In the present study Langmuir, Freundlich and Dubinin–Radushkevich models were tested for As(III) and As(V) adsorption.

Table 1 Pseudo-first and second order rate constants for sorption of As(V) and As(III) on the surface of Af-NPC/MnO_2 adsorbent at room temperature.

Elements	C_o	Pseudo first order rate parameters			Pseudo Second order rate parameters			
		q_e (mg/g)	K_1 (min^{-1})	R^2	q_e (mg/g)	K_2 (g/mg min)	h (mg/g min)	R^2
As(III)	1	1.51	3.43×10^{-2}	0.603	0.968	0.27×10^{-1}	2.362	0.999
	5	0.006	11.04×10^{-2}	0.807	4.672	1.7×10^{-1}	3.821	0.999
	10	0.24	7.3×10^{-2}	0.585	8.064	6.7×10^{-2}	4.57	0.998
As(V)	1	093	4.4×10^{-2}	0.621	0.992	5.1×10^{-1}	0.543	0.998
	5	0.026	6.2×10^{-2}	0.659	4.854	6.7×10^{-1}	2.289	0.998
	10	0.069	9.1×10^{-2}	0.476	8.488	5.6×10^{-1}	4.140	0.998

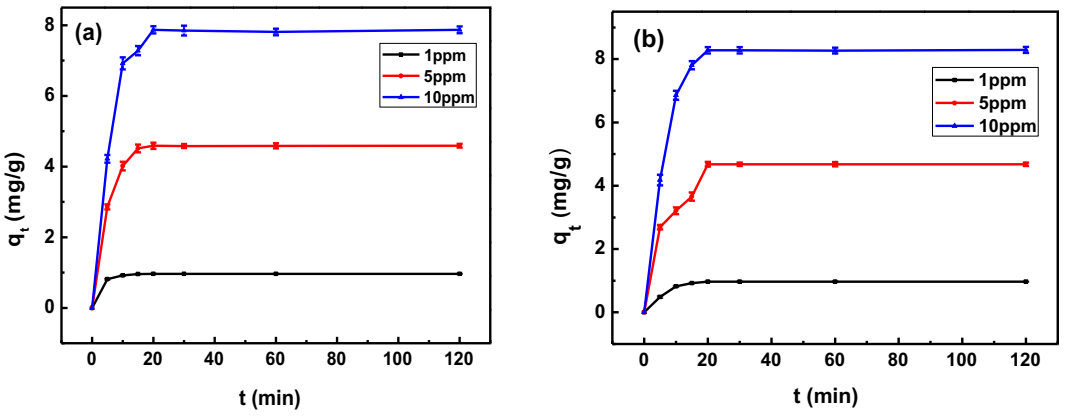

Figure 5 Time profile of (a) As(III) and (b) As(V) adsorption on Af-NPC/MnO_2 at various initial concentrations at pH 6 and room temperature.

Table 2 Summary of comparison of adsorption properties of Af-NPC/MnO_2 with other adsorbents reported in literature for removal arsenic.

Adsorbent	pH	Adsorption capacity (mg/g)		Initial Arsenic concentration (mg/L)	Equilibrium time (min)	Adsorbent dose (g/L)	Surface area (m^2/g)	References
		As(III)	As(V)					
Biomass waste derived activated carbon		–	1.01	20	60	2.5	258	Budinova et al. (2009)
Iron Oxide/Activated carbon	6	–	2.07	10	60	5	–	Yao et al. (2014)
Magnetite-doped activated carbon fibers	4	–	4.16	2	120	0.7	1392	Zhang et al. (2010b)
Chemically modified low cost adsorbent	6	0.085	0.083	0.5	30	0.15	–	Roy et al. (2013)
MnO_2-loaded polystyrene resin	–	0.7 mmol/g	0.3 mmol/g	–	120	2.3	–	Lenoble et al. (2004)
Iron Oxide Coated Multiwall Carbon Nanotubes	4	1.72	1.89	0.1	30	1	153	Ntim and Mitra (2011)
MnO_2/Alumina	7	42.48		300	120–180	5	194.09	Shihabudheen et al. (2009)
Af-NPC/MnO_2	6	8.85	9.43	10	15–20	1	633	This work

3.2.4.1. Langmuir and Freundlich isotherm. Langmuir isotherm is applicable to the homogeneous surfaces, which have equal adsorption affinity sites, while Freundlich model assumes heterogeneous adsorption sites. The linear form of Langmuir and Freundlich isotherms is described by Eqs. (6) and (7) respectively (Ntim and Mitra, 2011)

$$\frac{C_e}{q_e} = \frac{C_e}{q_m} + \frac{1}{K_L q_m} \tag{6}$$

$$\log q_e = \log K_F + \frac{1}{n} \log C_e \tag{7}$$

where K_L and q_m are the Langmuir adsorption constant (L/mg) and maximum monolayer adsorption capacity (mg/g) respectively. K_L represents affinity between solute and adsorbent. K_F and n are Freundlich constant (adsorption capacity) and adsorption intensity respectively. The other parameters are same as mentioned before. Fig. 6 shows adsorption isotherm plots based on measured data and Table 3 gives different parameters calculated from these two isotherms. Both the adsorption models are fitting well for arsenic adsorption. Langmuir Model fitted better to the adsorption as reflected by a high value of correlation coefficient, suggesting monolayer adsorption of arsenic on the surface of Af-NPC/MnO_2. Freundlich constant n was found to be 1.85 and 1.83 for As (V) and As(III) respectively which implies that adsorption of arsenic was favorable on the surface of Af-NPC/MnO_2. The bond energy also increases proportionally with surface density as n is more than 1. The maximum adsorption capacity by Langmuir model was found to be 8.85 and 9.43 mg/g for As (III) and As(V) respectively with initial concentration of 10 mg/L. Separation factor R_L was calculated by following equation.

$$R_L = \frac{1}{1 + K_L C_{0\max}} \tag{8}$$

C_{omax} is maximum initial concentration. The values of R_L, 0.024 and 0.039 imply that Langmuir isotherm is favorable ($0 < R_L < 1$). Hence based on isotherm study we can conclude that Af-NPC/MnO_2 could be an efficient adsorbent for

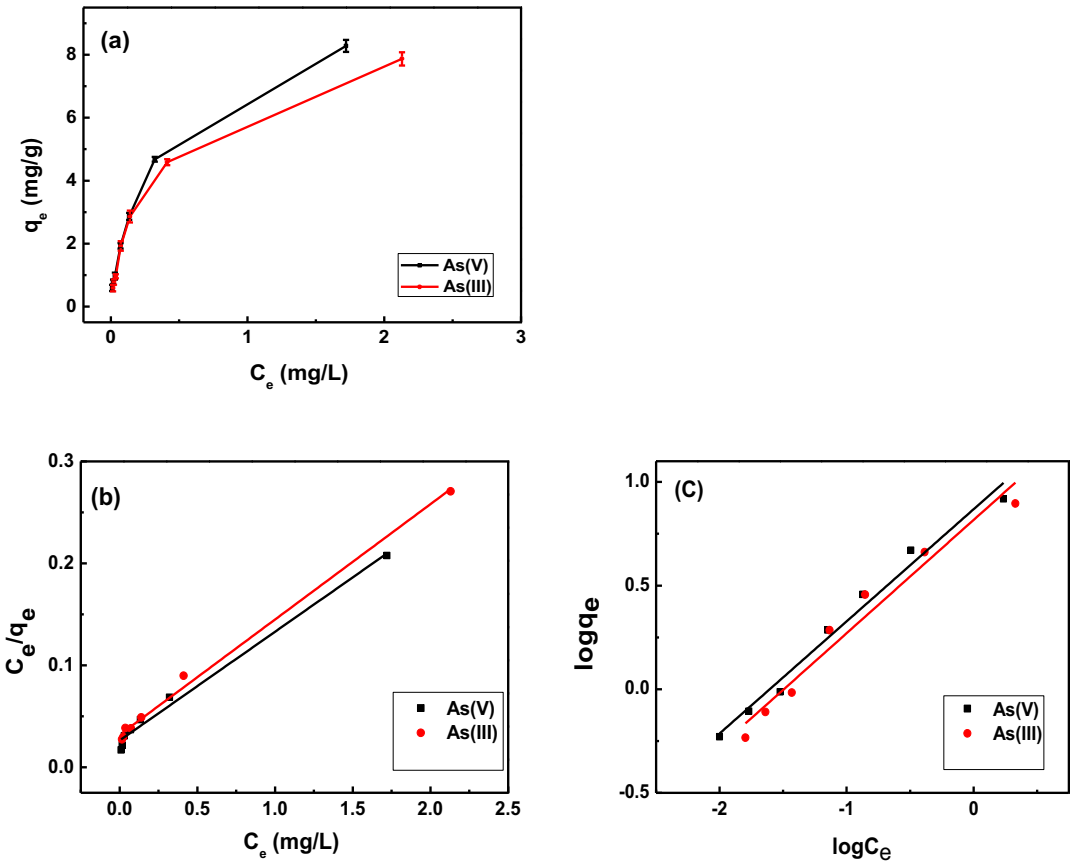

Figure 6 (a) Adsorption isotherm graph, (b) Langmuir isotherm plot and (c) Freundlich isotherm plot of As(V) and As(III) adsorption on the surface of Af-NPC/MnO_2 (Initial concentration of arsenic C_o = 0.6–10 mg/L).

Table 3 Langmuir and Freundlich isotherm parameters for As(III) and As(V) adsorption onto Af-NPC/MnO_2 adsorbent for initial concentration of arsenic between 0.6 and 10 mg/L.

Elements	Langmuir				Freundlich		
	q_m (mg/g)	K_L (L/mg)	R_L	R^2	K_F (mg/g)	n	R^2
As(III)	8.85	3.64	0.024	0.995	0.816	1.83	0.961
As(V)	9.43	4.081	0.039	0.99	0.868	1.85	0.981

removal of arsenic due to good affinity and adsorption capacity.

3.2.4.2. Dubinin–Radushkevich model (D–R). D–R model was used to determine nature of adsorption. The D–R model is represented by following equation (Hamideh and Majid, 2015).

$$\ln q_e = \ln q_m - \beta\varepsilon^2 \tag{9}$$

where β (mol^2 kJ^{-2}) is a constant related to mean adsorption energy and ε is the Polanyi potential which can be calculated from the following equation.

$$\varepsilon = RT\ln\left(1+\frac{1}{C_e}\right) \tag{10}$$

where T is the absolute temperature in Kelvin and R is the universal gas constant (8.314 Jmol^{-1} K^{-1}). C_e is concentration of arsenic ions at equilibrium in aqueous medium. The slope of plot of $\ln q_e$ versus ε^2 gives β (mol^2 kJ^{-2}) and the intercept yields the sorption capacity q_m (mg/g). The sorption energy or mean free energy E can also be calculated by using following relationship

$$E = \frac{1}{(2\beta)^{1/2}} \tag{11}$$

The value of mean free energy helps in understanding nature of bonding between adsorbate and adsorbent. Value of E less than 8 kJ/mol indicates physical adsorption and value between 8 and 16 kJ/mol implies chemisorptions (Hamideh and Majid, 2015). The adsorption data of arsenic fitted well to D–R model with regression values of 0.961 and 0.969 for

As(V) and As(III) respectively. Mean free energy E for As(V) and As(III) adsorption on the surface of Af-NPC/MnO_2 is 5 kJ/mol. Hence based on D–R isotherm adsorption of arsenic was physical on the surface of Af-NPC/MnO_2.

3.2.5. *Effect of interfering ions and adsorption efficiency in ground water sample*

Percentage removal efficiency of Af-NPC/MnO_2 reduces for As(V) and As(III) in the presence of NaCl and Na_2SO_4 (Fig. 7a and b). The presence of Cl^- and SO_4^{2-} ions decreases adsorption capacity of Af-NPC/MnO_2 due to competition between $H_2AsO_4^-$ and negatively charged ions (Cl^- and SO_4^{2-}) for active sites. Cl^- ions reduce adsorption capacity more compared to sulfate ions might be due to higher affinity and faster diffusion of Cl^- ions on the surface of Af-NPC/MnO_2 than SO_4^{2-} and $H_2AsO_4^-$ ions. Percentage removal efficiency of Af-NPC/MnO_2 for arsenic reduces only by 1–2% in ground water samples under same conditions of pH, temperature and rotation as compared to synthetic water (Fig. 7c).

3.2.6. *Sorbent regeneration*

Regeneration of any adsorbent is an important factor in the sorption process for reducing the overall cost of process. It was observed that 0.1 N NaOH could elute 89–95% of sorbed arsenic from Af-NPC/MnO_2. To test the reusability of regenerated adsorbent, the same sorbent was subjected to three consecutive cycles of adsorption–desorption. The results of these studies (Fig. 8) showed that Af-NPC/MnO_2 have good re-use potential and even at the third cycle the sorption efficiency was reduced only by 3–5%. However the adsorption efficiency of composite for both As(III) and As(V) investigated in the present study is still above 90% in third cycle. Maximum desorption was achieved in 20 min (Fig. 8c). From these results, it seems that Af-NPC/MnO_2 could be used as an effective alternative sorbent for arsenic removal. The ratio of volume of initially treated solution to the volume of NaOH solution used for desorption was 5.

3.3. *Mechanism of adsorption*

XPS results have shown the presence of As(V) on the surface of Af-NPC/MnO_2 after adsorption of both As(III) and As (V) from aqueous medium, which indicates that As(III) was oxidized to As(V) on the surface of composite. Shifts seen in FTIR spectra after adsorption of arsenic suggest involvement of oxygen containing groups during the process of adsorption. Moreover As(V) at pH 6 exists as $H_2AsO_4^-$ species. As surface of composite was negative at pH 6, anion exchange reactions seem to dictate mechanism of adsorption of $H_2AsO_4^-$ on the surface of Af-NPC/MnO_2. Decrease in adsorption of arsenic with increase in pH and the presence of other negative ions due to competitive adsorption supports that main mechanism of adsorption was anion exchanged reaction between $H_2AsO_4^-$ and —OH groups present on the surface of Af-NPC/MnO_2. Increase in pH from 6 to 6.5 after adsorption of arsenic was an indicator of release of OH^- ions in water.

As per pseudo second order rate the mechanism of adsorption was chemisorptions, but mean free energy from D–R

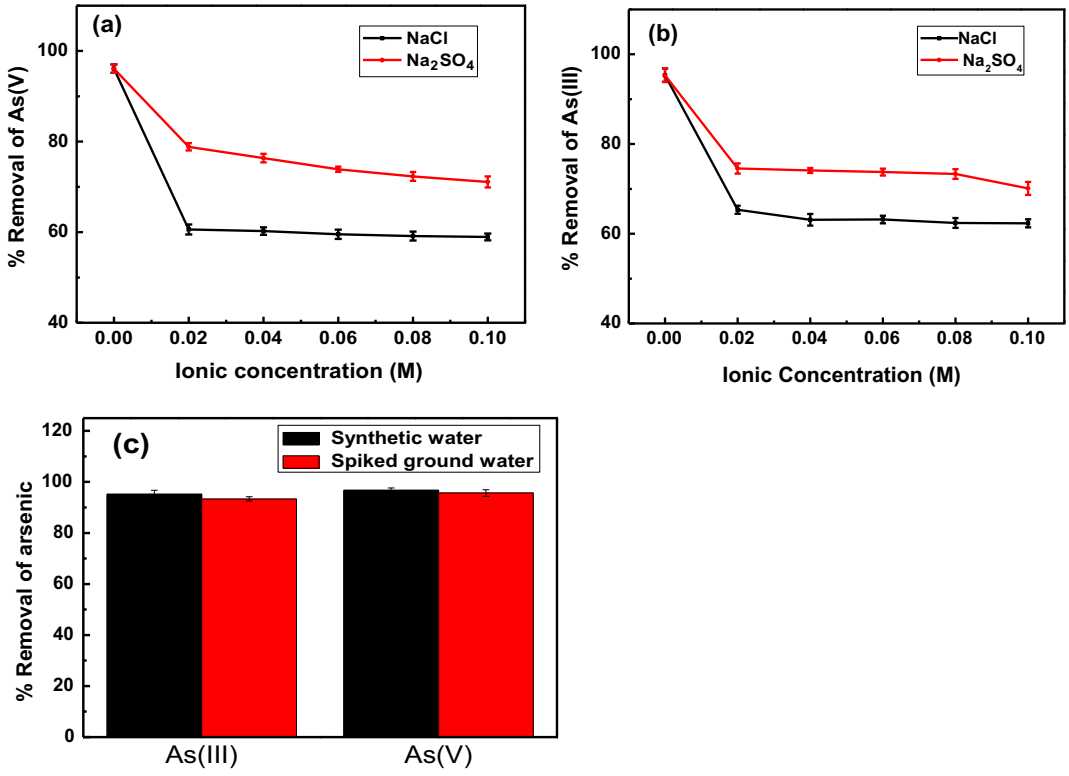

Figure 7 (a) and (b) Effect of salt concentration on % Removal efficiency of Af-NPC/MnO_2 for As(V) and As(III) respectively at pH 6 and room temperature, (c) % Removal of arsenic from spiked samples of ground water and synthetic water at pH 6 (Initial arsenic concentration = 1 mg/L).

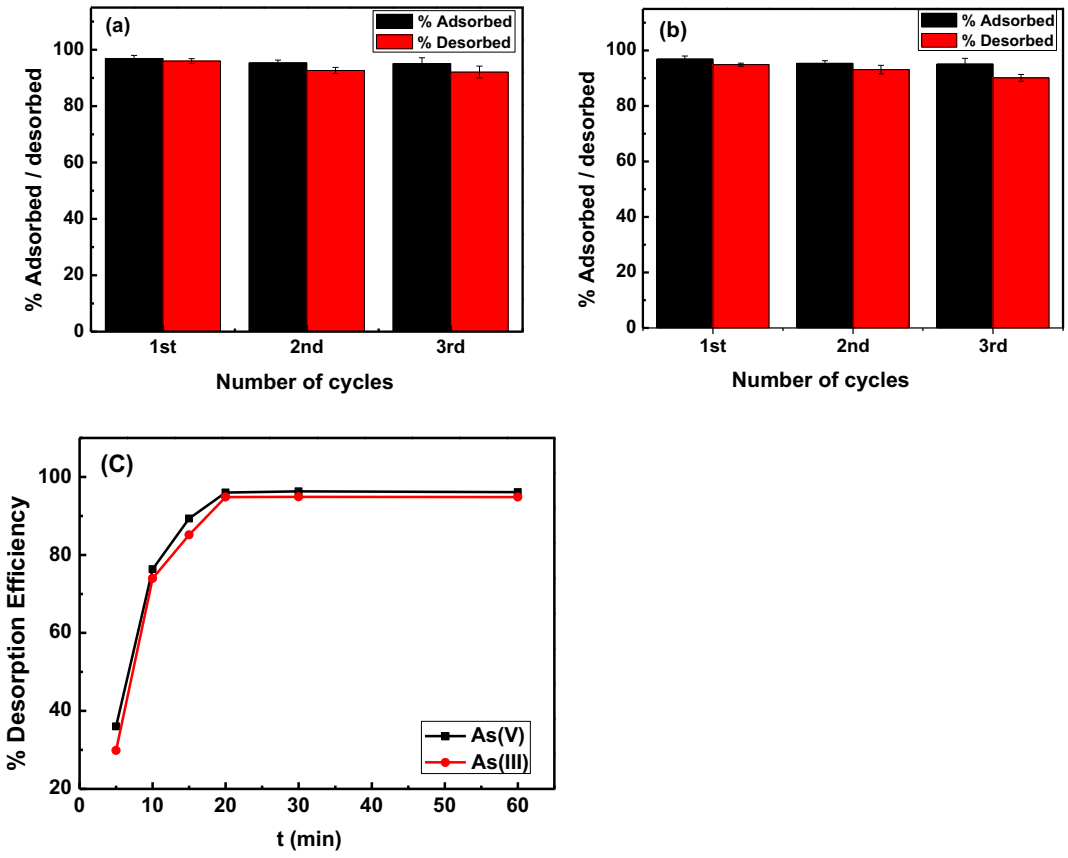

Figure 8 (a) and (b) % adsorption/desorption efficiency of Af-NPC/MnO_2 for As(V) and As(III) respectively during three consecutive cycles with initial arsenic concentration 1 mg/L. (c) Time profile for desorption of As(V) and As(III) by 0.1 N NaOH.

adsorption model implies that the process of adsorption was physical. Hence we can conclude from these findings that physicochemical interactions were involved during the process of adsorption of arsenic through anion exchange reaction on the surface of Af-NPC/MnO_2 (Eq. (12)).

$$\text{Af-NPC/MnO}_2\text{–OH} + \text{H}_2\text{AsO}_4^- \rightarrow \text{Af-NPC/MnO}_2\text{–H}_2\text{AsO}_4 + \text{OH}^- \quad (12)$$

4. Conclusion

Grass was found to be a good cost effective precursor for synthesis of nanoporous carbon. FTIR and XPS results have indicated formation of MnO_2 on the surface of Af-NPC in the synthesized composite. Study of adsorption property of Af-NPC/MnO_2 suggests that the synthesized composite is an efficient adsorbent for As(III) as well as As(V) over a wide pH range 4–6.5. The adsorption of arsenic on the surface of Af-NPC/MnO_2 follows second order kinetics with very fast removal rates in comparison with other adsorbents. Adsorption equilibrium for arsenic on the surface of Af-NPC/MnO_2 was reached within 15–20 min. Anion exchange reaction seems to dictate the mechanism of adsorption. The experimental equilibrium data fitted well in Langmuir isotherm model with maximum monolayer adsorption capacity of 8.85 mg/g and 9.43 mg/g for As(III) and As(V) respectively with initial concentration of 10 mg/L. Recycling studies showed that adsorbent can be easily used after regeneration with NaOH. The adsorption capacity reduces only by 3–5% up to third cycle of adsorption. The good adsorption capacity and fast removal rate imply that the synthesized composite has potential to be used as an efficient adsorbent for removal of arsenic from aqueous medium.

Acknowledgment

Authors are grateful to SAIF, Chemical Engineering department, ESCA and INUP, IIT Bombay, for providing instrumental facilities.

Appendix A. Supplementary material

Supplementary data associated with this article can be found, in the online version, at http://dx.doi.org/10.1016/j.arabjc.2016.12.011.

References

ATSDR, 2015. Priority List of Hazardous Substances.

Budinova, T., Savova, D., Tsyntsarski, B., Ania, C.O., Cabal, B., Parra, J.B., Petrov, N., 2009. Biomass waste-derived activated carbon for the removal of arsenic and manganese ions from aqueous solutions. Appl. Surf. Sci. 255, 4650–4657.

Chakraborti, D., Das, B., Rahman, M.M., Chowdhury, U.K., Biswas, B., Goswami, A.B., Nayak, B., Pal, A., Sengupta, M.K., Ahamed, S., Hossain, A., Basu, G., Roychowdhury, T., Das, D., 2009. Status

of groundwater arsenic contamination in the state of West Bengal, India: a 20-year study report. Mol. Nutr. Food Res. 53, 542–555.
De, S., Maiti, A., 2012. Arsenic Removal from Cantaminated Ground Water. The Energy and Resource Institute (TERI), New Delhi.
Driehaus, W., Seith, R., Jekel, M., 1995. Oxidation of arsenite(III) with manganese oxides in water treatment. Water Res. 29, 297–305.
Dutta, D., Thakur, D., Bahadur, D., 2015. SnO_2 quantum dots decorated silica nanoparticles for fast removal of cationic dye (methylene blue) from wastewater. Chem. Eng. J. 281, 482–490.
Giri, K.A., Patel, R.K., Mahapatra, S.S., Mishra, P.C., 2013. Biosorption of arsenic (III) from aqueous solution by living cells of *Bacillus cereus*. Environ. Sci. Pollut. R. 20, 1281–1291.
Gupta, V.K., Saini, V.K., Jain, N., 2005. Adsorption of As(III) from aqueous solutions by iron oxide-coated sand. J. Colloid Interface Sci. 288, 55–60.
Hamideh, K.M., Majid, P., 2015. Experimental study on mercury ions removal from aqueous solution by MnO_2/CNTs nano composite adsorbent. J. Ind. Eng. Chem. 21, 221–229.
Hristovski, K., Baumgardner, A., Westerhoff, P., 2007. Selecting metal oxide nanomaterials for arsenic removal in fixed bed columns: from nanopowders to aggregated nanoparticle media. J. Hazard. Mater. 147, 265–274.
Huang, M., Zhang, Y., Li, F., Zhang, L., Ruoff, S.R., Wen, Z., Liu, Q., 2014. Self-assembly of mesoporous nanotubes assembled from interwoven ultrathin birnessite-type MnO_2 nanosheets for asymmetric supercapacitors. Sci. Rep. 4, 3878.
Jiang, J.Q., 2001. Removing arsenic from groundwater for the developing world – a review. Water Sci. Technol. 44, 89–98.
Kamala, C.T., Chu, K.H., Chary, N.S., Pandey, P.K., Ramesh, S.L., Sastry, A.R.K., Chandra Sekhar, K., 2005. Removal of arsenic(III) from aqueous solutions using fresh and immobilized plant biomass. Water Res. 39 (28), 15–2826.
Lee, G.J., Pyun, S.I., 2007. Synthesis and characterization of nanoporous carbon and electrochemical application to electrode material for supercapacitors. Mod. Aspect Electroc. 41, 308.
Lee, T.T., Hong, J.R., Lin, W.C., Hu, C.C., Wu, P.W., Li, Y.Y., 2014. Synthesis of petal-like carbon nanocapsule@MnO_2 core-shell particles and their application in supercapacitors. J. Electrochem. Soc. 161, 598–605.
Lenoble, V., Laclautre, C., Serpaud, B., Deluchat, V., Bollinger, J.C., 2004. As(V) retention and As(III) simultaneous oxidation and removal on a MnO_2 –loaded polystyrene resin. Sci. Total Environ. 326, 197–207.
Lone, M.I., He, Z.L., Stoffella, P.J., Yang, X.E., Zhejiang, J., 2008. Phytoremediation of heavy metal polluted soils and water: progresses and perspectives. Univ. Sci. B 9, 210–220.
Meltem, B.B., Aysegul, P., 2014. Batch and fixed-bed column studies of arsenic adsorption on the natural and modified clinoptilolite. Water Air Soil Poll. 225, 1798.
Mishra, A.K., Ramaprabhu, S., 2011. Functionalized graphene sheets for arsenic removal and desalination of sea water. Desalination 282, 39–45.
Mohan, D., Pittman Jret, C.U., 2007. Arsenic removal from water/waste water using adsorbents – a critical review. J. Hazard. Mater. 142, 1–53.
Mojtaba, H., Nader, B., Habibollah, Y., Qin, L., 2014. Adsorption of mercury ions from synthetic and real wastewater aqueous solution by functionalized multi-walled carbon nanotube with both amino and thiolated groups. Chem. Eng. J. 237, 217–228.
Ntim, S.A., Mitra, S., 2011. Removal of trace arsenic to meet drinking water standards using iron oxide coated multiwall carbon nanotubes. J. Chem. Eng. Data 12, 2077–2083.
Patel, N., Fernandes, R., Gupta, S., Edla, R., Kothari, D.C., Miotello, A., 2013. Co-B catalyst supported over mesoporous silica for hydrogen production by catalytic hydrolysis of Ammonia Borane: a study on influence of pore structure. Appl. Catal. B: Environ. 140–141, 125–132.
Qu, Q.T., Zhang, P., Wang, B., Chen, Y.H., Tian, S., Wu, Y.P., Holze, R., 2009. Electrochemical performance of MnO_2 nanorods in neutral aqueous electrolytes as a cathode for asymmetric supercapacitors. J. Phys. Chem. 113, 14020–14027.
Roy, P., Mondal, N.K., Bhattacharya, S., Das, B., Das, K., 2013. Removal of arsenic(III) and arsenic(V) on chemically modified low-cost adsorbent: batch and column operations. Appl. Water Sci. 3, 293–309.
Shahin, A.P., Nancy, S.P., 2016. Nanoporous carbon synthesized from grass for removal and recovery of hexavalent chromium. Carbon Lett. 20, 10–18.
Shengsen, W., Bin, G., Andrew, R.Z., Yuncong, L., Lena, M., Willie, G.H., Kati, W.M., 2015. Removal of arsenic by magnetic biochar prepared from pinewood and natural hematite. Bioresource Technol. 175, 391–395.
Shihabudheen, M.M., Philip, L., Pradeep, T., 2009. As (III) removal from drinking water using manganese oxide-coated-alumina: performance evaluation and mechanistic details of surface binding. Chem. Eng. J. 153, 101–107.
Singh, S., Barick, K.C., Bahadur, D., 2011. Surface engineered magnetic nanoparticles for removal of toxic metal ions and bacterial pathogens. J. Hazard. Mater. 192, 1539–1547.
Smith, A.H., Arroyo, A.P., Mazumder, D.N., Kosnett, M.J., Hernandez, A.L., Beeris, M., Smith, M.M., Moore, L.E., 2000. Arsenic-induced skin lesions among Atacameño people in Northern Chile despite good nutrition and centuries of exposure. Environ. Health Perspect. 108, 617–620.
Sreeprasad, T.S., Maliyekkal, S.M., Lisha, K.P., Pradeep, T., 2011. Reduced graphene oxide – metal/metal oxide composites: facile synthesis and application in water purification. J. Hazard. Mater. 186, 921–931.
Thommes, M., 2010. Physical adsorption characterization of nanoporous materials. Chem. Ing. Tech. 82, 1059–1073.
Wagner, C.D., Riggs, W.M., Davis, L.E., Moulder, J.F., 1979. Handbook of X-Rayphotoelectron Spectroscopy. Perkin Elmer Cooperation.
Wang, G.X., Zhang, B.L., Yu, Z.L., Qu, M.Z., 2005. Manganese oxide/MWNTs composite electrodes for supercapacitors. Solid State Ionics 176, 1169–1174.
Wang, S.G., Gong, W.X., Liu, X.W., Yao, Y.W., Gao, B.Y., Yue, Q. Y., 2007. Removal of Pb(II) From aqueous solution by adsorption on to Manganese Oxide – coated carbon nanotubes. Sep. Purif. Technol. 58, 7–23.
Xiu, J.L., Liu, C.S., Li, F.B., Li, Y.T., Zhang, L.J., Liu, C.P., Zhou, Y. Z., 2010. The oxidative transformation of sodium arsenite at the interface of MnO_2 and water. J. Hazard. Mater. 173, 675–681.
Yao, S., Liu, Z., Shi, Z., 2014. Arsenic removal from aqueous solutions by adsorption onto iron oxide/activated carbon magnetic composite. J. Environ. Health Sci. Eng. 12, 58.
Zhang, S., Li, X.Y., Chen, J.P., 2010a. An XPS study for mechanisms of arsenate adsorption onto a magnetite-doped activated carbon fiber. J. Colloid Interface Sci. 343, 232–238.
Zhang, S., Li, X.Y., Chen, J.P., 2010b. Preparation and evaluation of a magnetite-doped activated carbon fiber for enhanced arsenic removal. Carbon 48, 60–67.